

An Analysis of the Processes Affecting Rapid Near-Surface Water Vapor Increases during the Afternoon to Evening Transition in Oklahoma

W. G. BLUMBERG,^{a,b,g} D. D. TURNER,^c S. M. CAVALLO,^a JIDONG GAO,^d J. BASARA,^{a,e} AND A. SHAPIRO^{a,f}

^a School of Meteorology, University of Oklahoma, Norman, Oklahoma

^b Cooperative Institute for Mesoscale Meteorological Studies, University of Oklahoma, Norman, Oklahoma

^c NOAA/Earth Systems Research Laboratory Global Sciences Division, Boulder, Colorado

^d NOAA/National Severe Storms Laboratory, Norman, Oklahoma

^e School of Civil Engineering and Environmental Science, University of Oklahoma, Norman, Oklahoma

^f Center for Analysis and Prediction of Storms, University of Oklahoma, Norman, Oklahoma

(Manuscript received 9 March 2019, in final form 9 August 2019)

ABSTRACT

This study used 20 years of Oklahoma Mesonet data to investigate the changes of near-surface water vapor mixing ratio q_v during the afternoon to evening transition (AET). Similar to past studies, increases in q_v are found to occur near sunset. However, the location, magnitude, and timing of the q_v maximum occurring during the AET are shown to be dependent on the seasonal growth and harvest of vegetation across Oklahoma in the spring and summer months. Particularly, the late spring harvest of winter wheat grown in Oklahoma appears to modify the relative contribution of local and nonlocal processes on q_v . By analyzing time series of q_v during the AET, it is found that the likelihood of a presunset q_v maximum is strongly dependent upon vegetation, soil moisture, wind speed, and cloud cover. Analysis also reveals that the increase in q_v during the AET can increase the parcel conditional instability despite the surface cooling produced by loss of insolation. Next to known changes in low-level wind shear, these changes in instability and moisture demonstrate new ways the AET can modify the presence of the key ingredients relevant to explaining the climatological increase in severe convective storm hazards around sunset.

1. Introduction

Land–atmosphere interactions operating on weather and climate scales are known to influence convective precipitation within the southern Great Plains (SGP) (e.g., Basara and Crawford 2002; Santanello et al. 2009, 2011, 2013, 2015; Wei et al. 2008; Ferguson and Wood 2011; Ford et al. 2015a,b,c; Ruiz-Barradas and Nigam 2013). During these interactions, the exchange of mass and energy between the land surface and atmosphere may induce various feedbacks that enhance or suppress deep, moist convection. The regional geography also plays a role in influencing SGP precipitation. Multiple studies of the Great Plains nocturnal low-level jet (NLLJ; e.g., Blackadar 1957; Bonner 1968; Stensrud 1996) have shown that it has a geographic dependence

(e.g., Holton 1967; Wexler 1961; Shapiro et al. 2016) and facilitates nocturnal convection and heavy rain events through water vapor transport and lifting (Means 1954; Pitchford and London 1962; Maddox 1980, 1983; Cotton et al. 1989; Stensrud 1996; Higgins et al. 1997; Arritt et al. 1997; Trier et al. 2006, 2014). Tied to this phenomenon is the climatological increase in thunderstorm-related hazards (e.g., precipitation, tornadoes) that begins in the evening hours (Means 1944; Wallace 1975; Orville 1981; Balling 1985; Mead and Thompson 2011). Although this increase has in part been explained by an increase low-level shear facilitated by the NLLJ (Maddox 1993; Coffey and Parker 2015; Mead and Thompson 2011; Bluestein et al. 2018), other hypotheses regarding changes beginning during the afternoon and evening to other ingredients such as lift or moisture (Doswell et al. 1996) that may complement this knowledge remain largely unexplored. Collectively, these studies suggest more knowledge is needed about the planetary boundary layer (PBL) over the diurnal cycle to help understand additional relationships between

^g Current affiliation: NASA Goddard Space Flight Center, Greenbelt, Maryland.

Corresponding author: Greg Blumberg, wblumberg@ou.edu

the land surface and deep, moist convection within the SGP.

To first order, the PBL can be divided into the convective or daytime boundary layers (CBL) and the stable or nighttime boundary layers (SBL; Stull 1988). The transition period between the CBL and SBL, however, that denotes the decay of dry convective, turbulent eddies can be divided even further into the evening transition (Lothon et al. 2014), the early evening transition (e.g., Mahrt 1981), the afternoon transition (Lothon et al. 2014), and the afternoon to evening transition (AET; Wingo and Knupp 2015). The definitions of these time periods vary from using astronomical sunset (Wingo and Knupp 2015) to changepoints in the surface sensible heat flux to denote their start and end times (Lothon et al. 2014). In this study, we focus on the AET: the 6-h period centered on local astronomical sunset. We use this definition as it helps normalize the observations taken during the evening by considering general changes in insolation and can facilitate comparisons across various past studies.

Regardless of the exact definition, investigators studying this transitional period have identified that the near-surface water vapor mixing ratio q_v tends to increase, sometimes at a very rapid rate ($\sim 0.1 \text{ g kg}^{-1} \text{ min}^{-1}$). Causes behind this change can be conceptualized using a simplified water vapor budget equation for flow following the ground:

$$\frac{\Delta \bar{q}_v}{\Delta t} = \frac{1}{\rho L_v} \frac{\text{LE}}{h} + \left(u \frac{\Delta \bar{q}_v}{\Delta x} + v \frac{\Delta \bar{q}_v}{\Delta y} \right) + Q. \quad (1)$$

Here, the local tendency of q_v can be described as a function of the local source (evapotranspiration; first term on the right-hand side) and a nonlocal source (horizontal advection; terms 2 and 3 in parentheses). In the local term, LE is the surface latent heat flux, h is the height of the top of the PBL, ρ is the air density, and L_v is the latent heat of vaporization. The evapotranspiration in this paper is considered to be the contributions from both evaporation off the surface and transpiration by plants. In the nonlocal terms, u and v represent the zonal and meridional wind components. The term Q indicates sources and sinks of water vapor caused by phase changes. Overbars indicate the mean component from Reynolds averaging. Note that we have assumed that the drying of the PBL via entrainment is negligible because we expect that mixing near the vertical gradient of water vapor at the top of the PBL will become small as convectively generated eddies decay throughout the transitioning CBL.

Research aimed at understanding which terms contribute to the observed changes of q_v during the AET

can be traced back to Fitzjarrald and Lala (1989) and Acevedo and Fitzjarrald (2001). In these papers, they identified several rapid jumps in q_v at observing sites deployed across the Hudson Valley region within New York State. These jumps were attributed to the rapid decay of turbulence occurring soon after the surface sensible heat flux became negative. An idealized large-eddy simulation described by Acevedo and Fitzjarrald (2001) showed how this local contribution could develop water vapor gradients along topographical variations that could be advected later on in the transition. Outside New York State, Busse and Knupp (2012) and Wingo and Knupp (2015) documented similar q_v changes in northern Alabama. Using a dataset of 140 cases, Wingo and Knupp (2015) demonstrated that the changes to q_v during the AET in northern Alabama are not limited to a particular season. Their analysis was the first long-term observational study to indicate these changes and suggested that the observed jumps were caused by evapotranspiration. To date however, only Bonin et al. (2013) have focused on the AET in the SGP, where they documented two cases of a rapid q_v increase using an uncrewed aerial vehicle (UAV). An analysis of the UAV data suggested that similar to the studies in the Hudson Valley and northern Alabama, the SGP q_v changes were due to evapotranspiration. In general, these studies indicate that local contributions are important in generating the changes of q_v during the AET.

Studies of changes to near-surface water vapor across Oklahoma during the AET tend to focus on a reversal of the motion of the dryline, which is a sharp moisture boundary found often in the SGP warm season (Fujita 1970; Schaefer 1974; Bluestein et al. 1988, 1989; American Meteorological Society 2019). This reversal of motion suggests that moisture changes in the SGP during the AET are driven by transport instead of from a local source. This line of thought is reinforced by debate as to whether or not retreating dryline motion may best be modeled as a density current (Parsons et al. 1991; Crawford and Bluestein 1997). However, detailed surface analyses indicate that drylines may have multiple moisture gradients when retreating and may exhibit “both continuous motion and redevelopment” (Hane et al. 2001, 2002; Hane 2004). These observations suggest that dryline behavior during the AET cannot be explained by advection alone. When read together, it appears possible that the studies showing localized AET moisture jumps and SGP dryline motion could be unified to explore where these two lines of inquiry overlap. Such work may reveal how AET processes impact the mesoscale evolution of drylines.

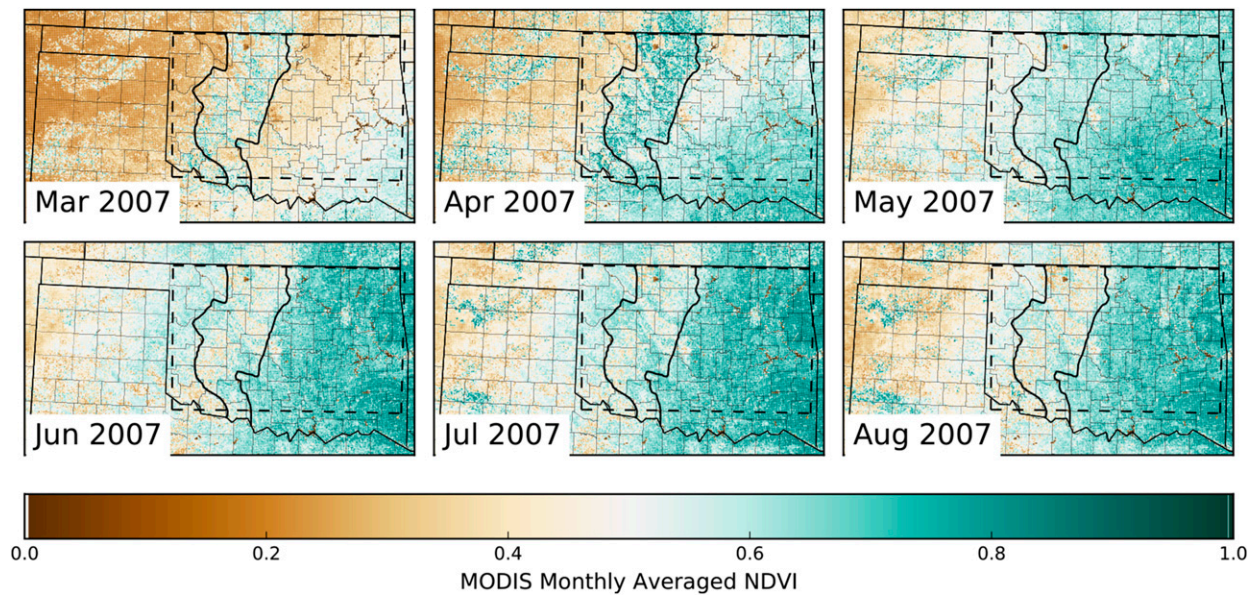


FIG. 1. Monthly averages (March–August) during 2007 of the MODIS-derived NDVI for the SGP. The area between the two solid black lines denotes the location of the WWB within Oklahoma from McPherson et al. (2004), which focused primarily on the changes within Oklahoma. The black dashed lines indicate the boundaries of the analysis domain described in section 2 and seen in Fig. 2.

A starting point for exploring these two lines of inquiry may be to first consider where evapotranspiration plays a role in the spatial moisture distribution in Oklahoma (e.g., Johnson and Hitchens 2018). One such location highlighted by past studies is the Great Plains winter wheat belt (WWB; e.g., Rabin et al. 1990). Winter wheat is typically sown in autumn and harvested in late May or early June (Loveland et al. 1995; McPherson et al. 2004; Haugland and Crawford 2005; Bagley et al. 2017). These shifts in the land surface properties are easily monitored using the normalized difference vegetation index (NDVI) product produced by satellite observations (Fig. 1). During March and April, the winter wheat is a distinct band of vegetation in Oklahoma. As the months progress, the native grasslands surrounding the WWB grow. By the beginning of June, the harvest of the winter wheat crop can be seen by the drop in NDVI in the WWB region relative to the surrounding areas. When combined with past observations and studies, the evolution shown in Fig. 1 appear to be representative of the location and timing of seasonal changes to the Oklahoma land surface going back to at least the 1980s (e.g., Rabin et al. 1990; Loveland et al. 1995).

Studies of the influence the WWB has on the atmosphere can be traced back to the Preliminary Regional Experiment for STORM-Central (PRE-STORM, where STORM is short for Storm-Scale Operational and Research Meteorology; Markowski and Stensrud 1998). During this experiment, a mesonet network of surface

observations showed how the winter wheat harvest was a clear factor in modifying the surface layer diurnal cycle. This result was revisited by McPherson et al. (2004) and Haugland and Crawford (2005) using Oklahoma Mesonet data. They too showed that the WWB may cause large dewpoint and temperature anomalies relative to the surrounding vegetation over the diurnal cycle. Further support to this hypothesis was found using numerical weather prediction simulations that artificially removed WWB vegetation from the land surface model (McPherson and Stensrud 2005). Because these studies focused on the general impact the WWB has over the diurnal cycle, they did not focus on the changes occurring during the AET and therefore did not discuss possible links to past AET-focused studies.

2. Study method and datasets

This study sought to explore the water vapor changes occurring during the Oklahoma AET by better understanding its causes and implications. Three questions are addressed:

- 1) What is the spatiotemporal evolution of q_v in Oklahoma during the AET?
- 2) What processes cause these changes in q_v and what environmental cues can be used to predict the likelihood of them?
- 3) How do these changes impact the conditional instability of near-surface parcels?

To answer these questions, we use two decades of surface meteorological data combined with analysis strategies (sections 2b,c) structured around the methods found in Acevedo and Fitzjarrald (2001), Wingo and Knupp (2015), McPherson et al. (2004), and Haugland and Crawford (2005).

a. The Oklahoma Mesonet

Data collected by the Oklahoma Mesonet (or simply the Mesonet) are used to characterize the Oklahoma near-surface AET. The Mesonet consists of 121 observing stations across Oklahoma and is managed by Oklahoma State University, the University of Oklahoma, and the Oklahoma Climatological Survey (Brock et al. 1995; McPherson et al. 2007). The q_v was derived by using measurements of temperature, relative humidity, and pressure at each Mesonet station. To characterize the environment, each site's anemometer, downwelling-shortwave pyranometer, and soil heat dissipation sensors were used. The anemometer was used to characterize the ambient wind speed, and the shortwave pyranometer was used to characterize the cloud cover. Last, the fractional water index (FWI) was derived from the soil moisture sensor to approximate the magnitude of evapotranspiration from the surface (Illston et al. 2008; Johnson and Hitchens 2018). FWI varies between values of 0 (very dry) and 1 (very wet and soil is at field capacity).

Only data collected in the meteorological spring and summer months (March–August) between 1994 and 2014 were used. There were 3822 AET events during this 20-yr period with at least 114 Mesonet sites operational per event. This dataset has around 600 AET cases to analyze for each month considered. With the exception of the FWI measurements (taken every 30 min), the temporal sampling rate of the Mesonet data is 5 min. The data were reported in coordinated universal time (UTC), but the time relative to astronomical sunset was calculated using the PyEphem software code (Rhodes 2011; <https://rhodesmill.org/pyephem/index.html>) to better compare with past studies. Satellite-based NDVI observations of Oklahoma provided by this study (e.g., Fig. 1) and past studies (e.g., Markowski and Stensrud 1998; McPherson et al. 2004) strongly indicate that the evolution of vegetation across Oklahoma is consistent across every year of this 20-yr dataset. By using a long record of data with consistent land surface changes between March and August, the signal of the land surface's influence on the AET could be extracted.

To characterize the cloud cover of each Mesonet time series, the difference between the observed downwelling shortwave flux and the expected radiation computed for a cloud-free sky was analyzed. To calculate

the expected radiation, a simple model outlined in Stull (1988) from Zhang and Anthes (1982) was used. Using our algorithm, each time series was classified as having clear sky, scattered clouds, or overcast clouds. For each month, subjective thresholds were used to detect these categories by analyzing the difference between the AET-daytime (3 h prior to sunset) observed and theoretical downwelling shortwave flux of 3000 randomly chosen time series. For each time series, the average differences and the logarithm of the standard deviation of the differences were calculated. When both the average differences and the variability of the differences were low, the AET was considered to be cloud free. If the variability was high but the average differences were low, the AET tended to display scattered clouds. When both the average difference and the variability were high, the AET was considered to have overcast skies. Comparisons with Geostationary Operational Environmental Satellite (GOES) visible imagery for several cases suggested that this cloud-detection logic correctly characterized the ambient cloud cover at the beginning of each AET.

b. 2D-VAR

A two-dimensional variational analysis (2D-VAR) program was run using a 12-km rectilinear grid (Fig. 2) with the Oklahoma Mesonet data to produce surface analyses every 5 min. The 2D-VAR algorithm was chosen since it more accurately reproduces both scalar fields and their spatial derivatives compared to other common objective analysis methods (Spencer et al. 2003; Spencer and Gao 2004). The 2D-VAR minimizes a cost function that compares the analysis and scalar observations and derived gradient “observations.” While the scalar observations used were from the Mesonet stations, the gradient observations were calculated by performing a Delaunay triangulation (Fig. 2) on the station observations, and by calculating the gradient at each triangle centroid (Spencer and Doswell 2001). 2D-VAR uses an additional tuning parameter Ψ in the cost function, which determines the relative weight between the scalar and gradient observations when performing the minimization. During the minimization process, a recursive filter spreads the adjustments made by each observation to nearby grid points. The horizontal correlation scale for this filter was roughly 120 km (Purser et al. 2003).

Prior to generating analyses on the Mesonet data, 2D-VAR was calibrated to maximize the accuracy of the water vapor analyses. Similar to the calibration method performed in Spencer and Gao (2004), simulated observations sampled from a truth grid were analyzed using multiple runs of 2D-VAR, each with a

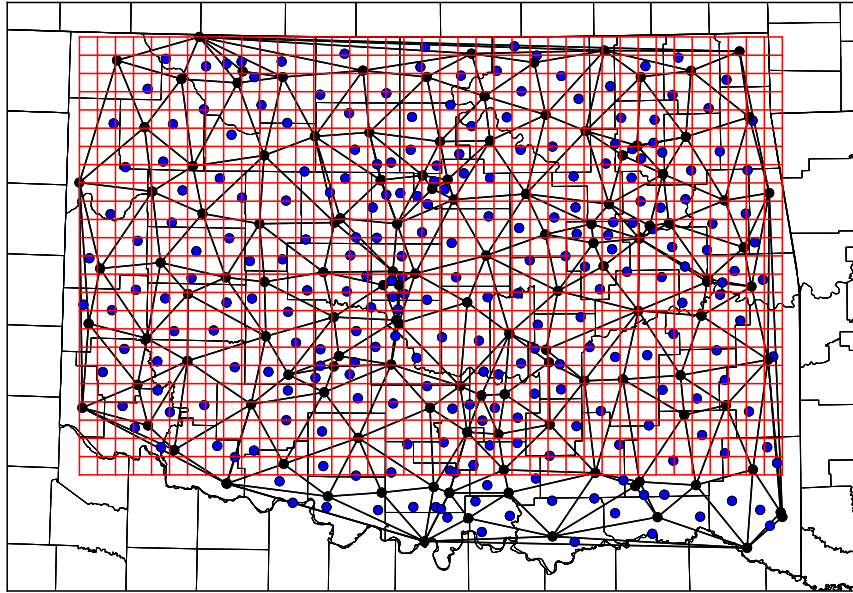


FIG. 2. The 12-km 2D-VAR grid (red) relative to the scalar observations from the Oklahoma Mesonet (black) and the gradient observations derived from those points (blue). Delaunay triangulation was used to develop the individual triangles (outlined with black lines) used to calculate the gradient observations.

different Ψ value. Each run of 2D-VAR was then compared with the truth grid to determine the Ψ value that best reproduces the original field. For this study, 90 randomly selected 20-km Rapid Update Cycle (RUC; Benjamin et al. 2004) model output grids between April 2002 and October 2003 were used to provide a wide variety of conditions for which to calibrate 2D-VAR. Each grid was interpolated to the 2D-VAR 12-km grid, and temperature, relative humidity, pressure, and wind observations similar to those taken by the Oklahoma Mesonet sites were created using bilinear interpolation.

Three variables (q_v , ∇q_v , and horizontal advection of q_v) were calculated from the 2D-VAR analyses and truth grids in the calibration step (Fig. 3). During this step, the accuracy of both the q_v and the magnitude of its horizontal gradient field (∇q_v , computed via finite differencing from the q_v field) were found to increase as the 2D-VAR Ψ parameter increases (Figs. 3a,b). For these two fields, 2D-VAR runs using a Ψ greater than or equal to 10^{10} best reproduced the truth fields. Horizontal water vapor advection was then calculated by using the horizontal gradient of q_v and horizontal components of u and v from 2D-VAR analyses of Mesonet observations. When horizontal q_v advection is considered, there is a clear range of values for which the analysis errors are minimized (10^{10} – 10^{12}) (Fig. 3c). Because of the error characteristics of the three fields considered in Fig. 3, the Ψ parameter was

set to 10^{10} when running 2D-VAR on the observed Mesonet data.

c. AET extrema analysis

The changes during the AET were also examined by analyzing Oklahoma Mesonet data to better understand the times when maxima in the near-surface water vapor, conditional instability, and virtual temperature occur. As our dataset only provides surface properties, changes in conditional instability are inferred by analyzing changes in equivalent potential temperature θ_e calculated from the surface data (Bolton 1980). Each time series was temporally interpolated to a 5-min grid centered on local sunset. Each interpolated time series of the AET from the Oklahoma Mesonet were grouped into the three land surface regions relative to the WWB used in McPherson et al. (2004). These regions are called the west WWB (W-WWB), the WWB, and the east WWB (E-WWB) (Fig. 4).

These three regions represent three distinct land surface types that undergo seasonal shifts in land surface properties each year. These groups span across a climatological west–east soil moisture gradient that has been the subject of several land–atmosphere coupling studies in the SGP (Illston et al. 2004; Ford et al. 2015a,b,c; Basara and Christian 2018; Wakefield et al. 2019; Basara et al. 2019). In comparison with the other two groups, the W-WWB region has the highest elevation

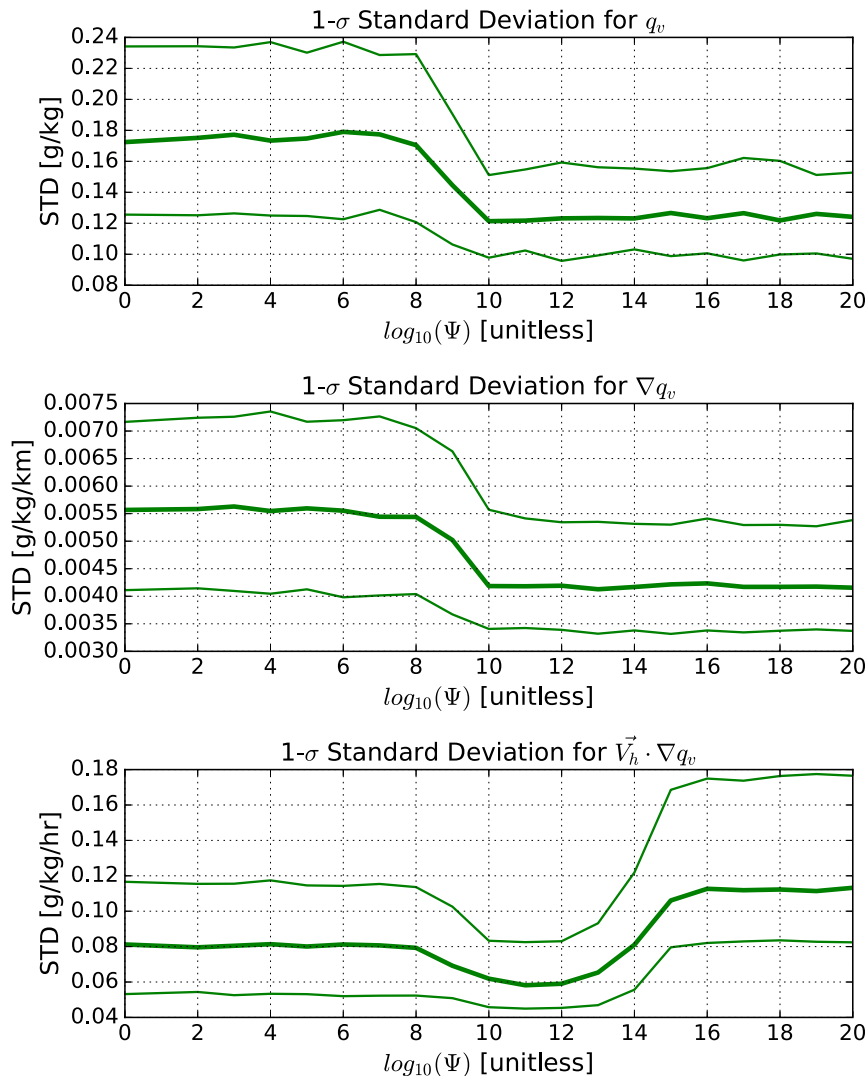


FIG. 3. Results from the calibration of the 2D-VAR algorithm discussed in section 3. Plots indicate the 1-sigma standard deviation of the error for all grid points for (a) q_v , (b) the magnitude of the gradient of q_v , and (c) the horizontal q_v advection. The thick, green solid line indicates the median statistic while the thinner green lines indicate the 25–75th percentiles.

and the lowest climatological soil moisture values. The WWB region lies in a region of lower elevation and is wetter with seasonal crops. Irrigation is not used to help grow the crops within the WWB. The E-WWB region is typically wetter than the W-WWB. This region represents the lowest elevation and primarily hosts vegetation that is native to the area.

The Mesonet time series were used to develop probability density functions (PDF) describing at what time a variable (e.g., q_v) for each region most likely reaches its maximum value. Because each land surface group contains several thousand AET cases, the following resampling procedure of the AET time series was used to generate confidence intervals of the PDFs. For each land surface group,

500 AET time series were randomly drawn 1000 times with replacement. For each of the 500 samples, the PDF was estimated using the SciPy software Gaussian kernel density estimator (Jones et al. 2001), which uses Scott's rule to determine the bandwidth of the estimator (Scott 2015). From the 1000 PDFs, the mean PDF and 2-sigma uncertainties were calculated to assess whether the 95% confidence intervals between the different land surface groups overlap. When testing for the sensitivity to these probabilities to environmental conditions, the 1000 PDFs were integrated over the 1.5 h prior to sunset to capture how likely a maximum is reached in the presunset hours. This method harnesses the vast Mesonet dataset to increase the statistical power in our analysis.

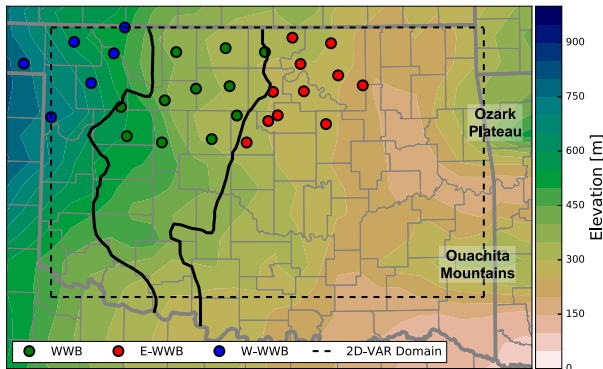


FIG. 4. A map of Oklahoma showing the categorized Mesonet sites relative to the WWB borders used in McPherson et al. (2004) (solid black lines). W-WWB and E-WWB refer to the sites west (blue) and east (red) of the WWB (green). In the background is a coarse relief map at 0.25° spacing to illustrate the geographical features discussed in the text. The box denoted by the dashed black line indicates the 2D-VAR analysis domain.

3. Water vapor changes during the AET

Initial analysis of q_v provided by 2D-VAR was used to answer the first question regarding the spatiotemporal evolution of water vapor during the AET. The data for each month were analyzed using analysis methods outlined in sections 2b and 2c. Maps showing the median change of q_v relative to the value found at the start of the AET were created for each month, similar to the analysis method used in Wingo and Knupp (2015) (Fig. 5). These maps were created with the expectation that distinct changes would coincide with the growth and harvest of WWB vegetation (Fig. 1).

Several similarities exist between the trends in Fig. 5 and the results of the Wingo and Knupp (2015) study. First, the magnitude of the changes in q_v that occur during the AET tend to be larger in the summer (June–August) than the spring (March–May) (Fig. 5, from top row to bottom row). In our data, the magnitude of the q_v changes increases from month to month and in particular along the WWB in the spring months. Second, the start times of the q_v increase between the two studies are similar—both begin approximately 1.5 h prior to sunset. Third, the increase in q_v persists after sunset in both studies; however, our data show that this only occurs in the summer months. Last, the q_v changes we find are on the same order of magnitude (1 g kg^{-1}) as those found in Wingo and Knupp (2015) as well as Bonin et al. 2013.

Unique to this study is that the q_v changes during the AET can be linked to the land surface, and in particular with the vegetation changes from month to month in

Fig. 1. As mentioned previously, the increases seen in Fig. 5 tended to be located within the WWB during the presunset hours of the spring months. After the WWB harvest, increases occur within the WWB, but they occur primarily after sunset (see June). In the summer months, the changes in q_v are larger and are generally concentrated east of the WWB where actively growing vegetation is present per Fig. 1. In eastern-central Oklahoma, an isolated maximum in q_v develops during the summertime AET (Fig. 5, June–August) in the valley between the Ozark Plateau and Ouachita Mountains (see Fig. 4). This topographical feature was shown to be a favorable location for increases in q_v by a large-eddy simulation of the AET in Acevedo and Fitzjarrald (2001).

Analysis of the PDFs illustrating the times a maximum value of q_v is reached during the AET builds further confidence that the AET has as strong dependence on the land surface properties. For March and April (Fig. 6), the E-WWB and W-WWB have very similar PDFs, and both climatologically have very little actively growing vegetation (Fig. 1). In contrast, the WWB has three peaks in the March and April PDFs, starting at the beginning of the AET, the end of the AET, and about a half hour prior to sunset. This final peak approximates the likelihood of a presunset q_v jump and is a key feature that will be discussed more in the subsequent sections. The probability of this feature increases as the months progress between March and May within the WWB region. In May, the E-WWB PDF shifts from looking similar to the W-WWB to the WWB. This shift coincides with the growth of native vegetation in the E-WWB in Fig. 1.

A shift of the WWB PDF occurs once the WWB is harvested between May and June (Fig. 6) and further indicates the AET's dependence on the land surface. Now, the WWB PDF appears similar to the W-WWB PDF while the E-WWB stays consistent (June–August). The probability of the presunset q_v jump also increases slightly for the E-WWB region between May and June. For the summer months, the WWB and W-WWB PDFs indicate that the likelihood of a maximum of q_v increases starting at roughly 1.5 h prior to sunset before ending at the end of the AET, which is consistent with the persistent increases throughout the AET in these locations shown in Fig. 5. An important result is that the uncertainty ranges generated by bootstrapping the PDFs in Fig. 6 demonstrate that the distinct differences in the three regions and their shifts in behavior do not appear by chance. The land surface dependency shown by this analysis motivates the next section to investigate the processes that facilitate q_v changes during the AET.

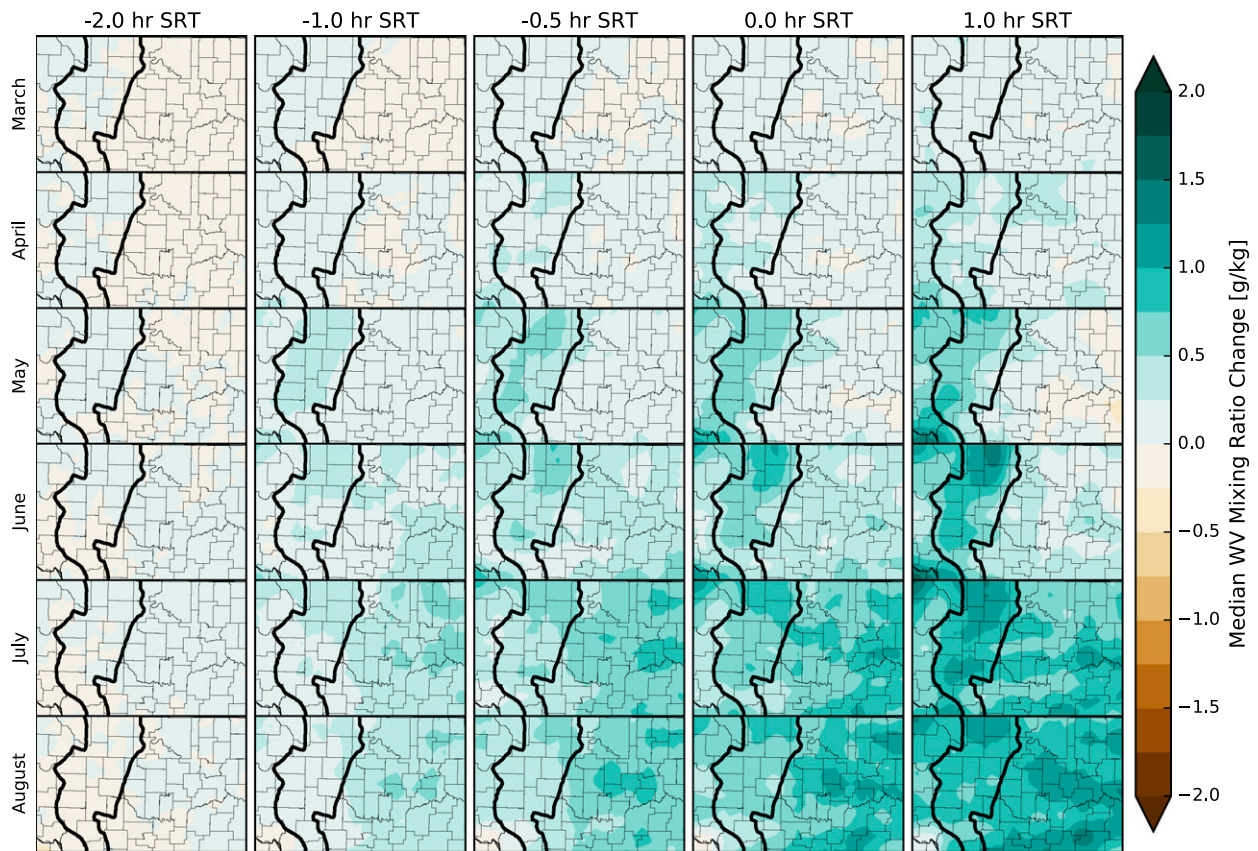


FIG. 5. Median change in q_v relative to the value measured at the start of the AET. Rows correspond to 2D-VAR data from the months March–August, and columns refer to the time of the map in SRT. The two black lines indicate the outline of the WWB from McPherson et al. (2004).

4. AET q_v processes and environmental parameters

Given the results in section 3, the data were analyzed in an attempt to understand the processes creating the observed changes in q_v . To do this, both the 2D-VAR and maxima analysis datasets discussed in section 2 were used along with the simplified water vapor mixing ratio budget equation [Eq. (1)] to isolate the processes and their dependencies.

a. WWB harvest impact on AET water vapor budget

Using the 2D-VAR dataset, the individual terms of the simplified water vapor budget equation were estimated. The diabatic term [Q in Eq. (1)] was first found to be relatively unimportant as the distribution of relative humidity values from the 2D-VAR analyses tended to only approach saturation near the end of the AET (not shown). In fact, only about 10% of the cases showed relative humidity values above 90% late in the AET. Therefore, focus was shifted to calculating the other terms. The term on the left-hand side of Eq. (1)—the local rate of change of q_v over time—was calculated

using centered finite differencing. Next, the horizontal q_v advection was calculated using the method outlined in section 2b. Last, by subtracting the local tendency term from the advection term a residual was computed and may be considered to be an estimate of the local contribution from evapotranspiration. Using this analysis, the 2D-VAR analyses reveal how the changes in land surface properties affect which processes cause q_v to change during the AET.

In the month of May, immediately prior to the harvest of the WWB, q_v advection plays little to no role modifying q_v during the AET. The q_v advection values in May are most often between $\pm 0.1 \text{ g kg}^{-1} \text{ h}^{-1}$ (Fig. 7, middle row). The local tendency of q_v is positive throughout the western half of the state and depicts that an increase in q_v occurs during the AET, similar to Fig. 5. The largest values of this term can be found within the bounds of the WWB about 1 h before sunset (Fig. 7, top row). Because advection is small, much of the q_v changes are attributable to evapotranspiration, as seen by the residual term (Fig. 7, bottom row). Additional evidence for this conclusion is that these increases occur within the WWB during May, when the wheat has reached maturity.

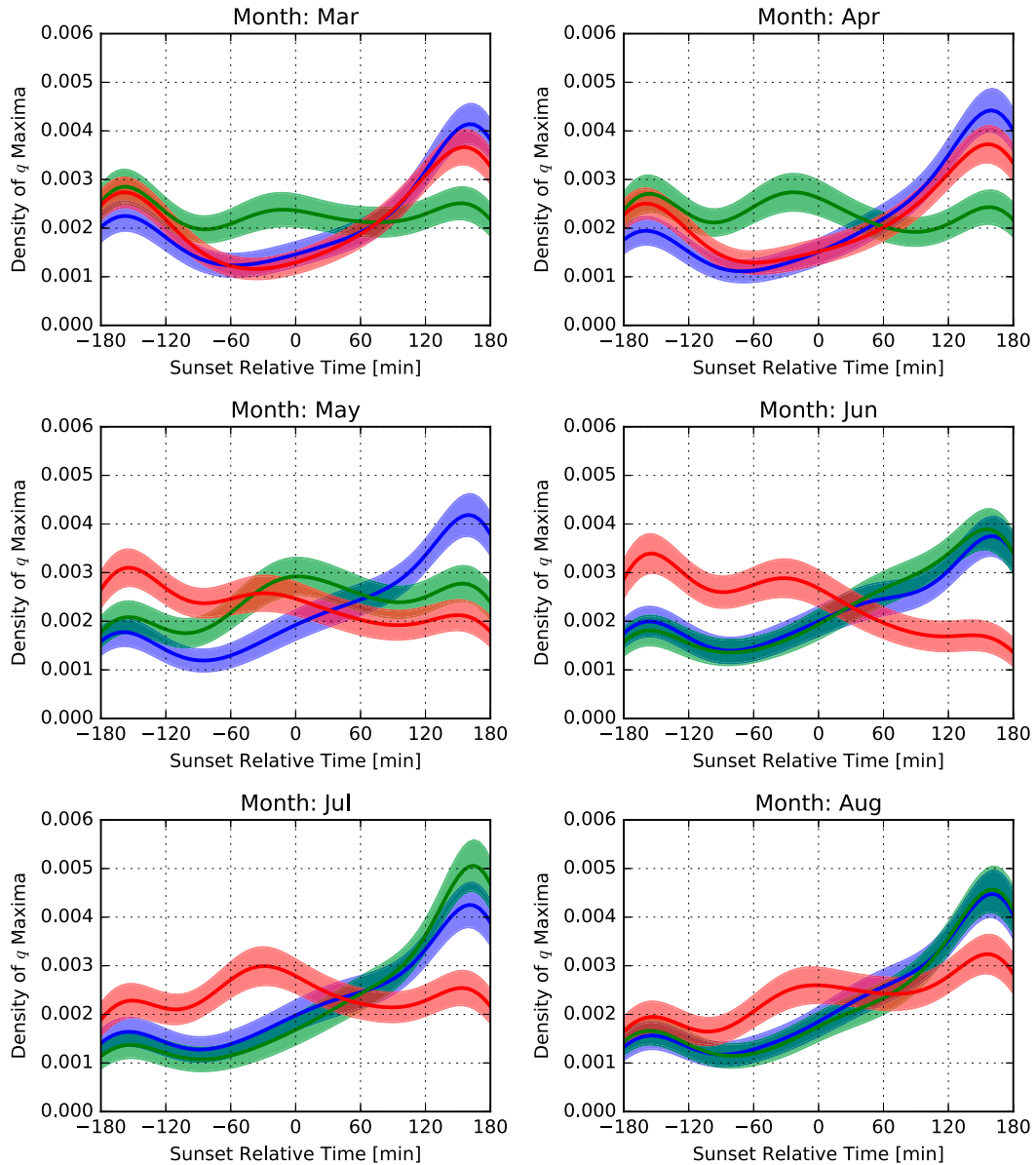


FIG. 6. Monthly bootstrapped PDFs indicating the time of the maximum q_v during the AET relative to astronomical sunset. Blue indicates sites in the W-WWB category, green indicates the sites within the WWB, and red shows the sites in the E-WWB category. The shaded regions indicate the 95% confidence intervals calculated with the bootstrapping method.

Similar conclusions are found in maps created for April and March (not shown), although the increases in q_v are weaker.

After the harvest, changes occur in how the local and nonlocal processes contribute to q_v changes. These changes are illustrated best in maps for the month of July. As was seen in Fig. 5, the increases in q_v are stronger during the AET in July than those found in May (top rows, Figs. 7 and 8). These changes are strongest east of the WWB ($0.3\text{--}0.5\text{ g kg}^{-1}\text{ h}^{-1}$) and occur during the hours

prior to sunset. However, early during the AET within the WWB the local tendency of q_v term appears close to zero (top row). The advection and the residual terms have sharp changes, particularly within the WWB. Between 1 and 2 h prior to sunset, the residual term (Fig. 8, bottom row) undergoes a reversal from negative to positive within the WWB, while the area east of the WWB remains largely positive for much of the AET. Moist advection on the order of $0.1\text{--}0.3\text{ g kg}^{-1}\text{ h}^{-1}$ is also now present within the WWB throughout the AET—a consequence of

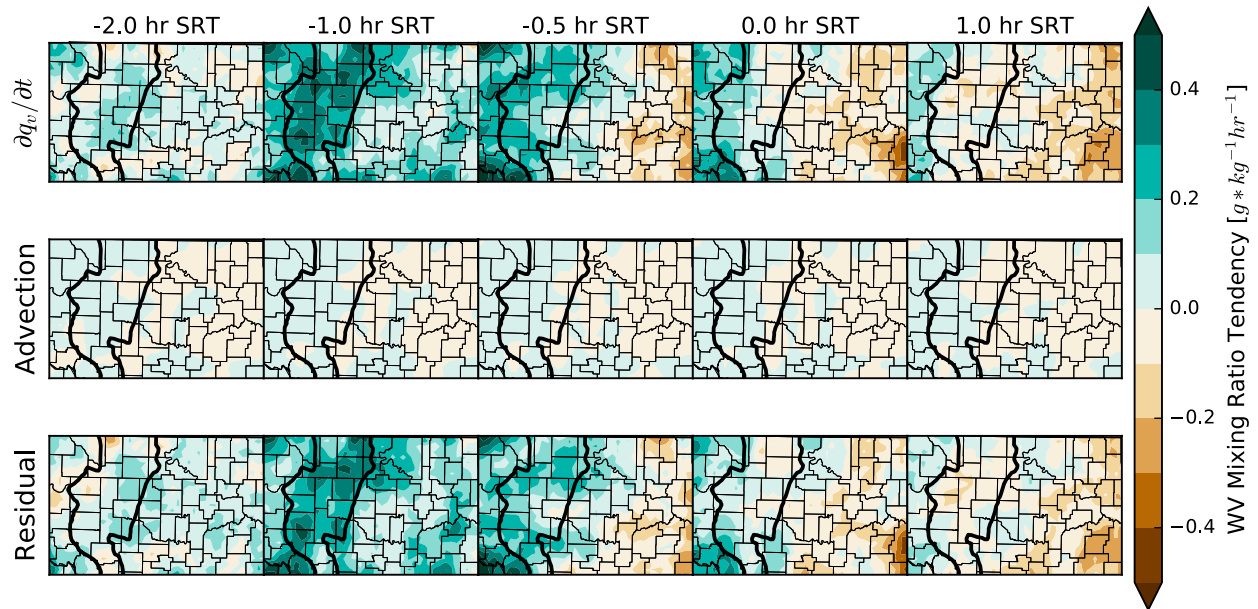


FIG. 7. Estimated median values from 2D-VAR using the water vapor tendency equation for May: (top) the tendency at each point of the grid of q_v , (middle) the horizontal advection of q_v , calculated from the 2D-VAR grid (the nonlocal contribution), and (bottom) an estimate of the local contribution to q_v by evapotranspiration, which is the residual taken by subtracting the top row from the middle row.

easterly winds and a moisture boundary that is oriented north to south, much like a dryline (Fig. 8, middle row). Based upon the zonal gradient in the residual term on the eastern edge of the WWB [-2 h sunset relative time (SRT), bottom row], it appears that the advected moisture gradient that develops along the WWB is a consequence of differential evapotranspiration during the

daytime. As this gradient is not seen in the preharvest months, these differences in AET evolution appear to be driven by the spatial contrasts in land surface properties brought on by the harvest of the WWB.

Reflection on the varying contributions between local and nonlocal sources of q_v lends to some additional thoughts on the causes and behavior of AET q_v . First, we

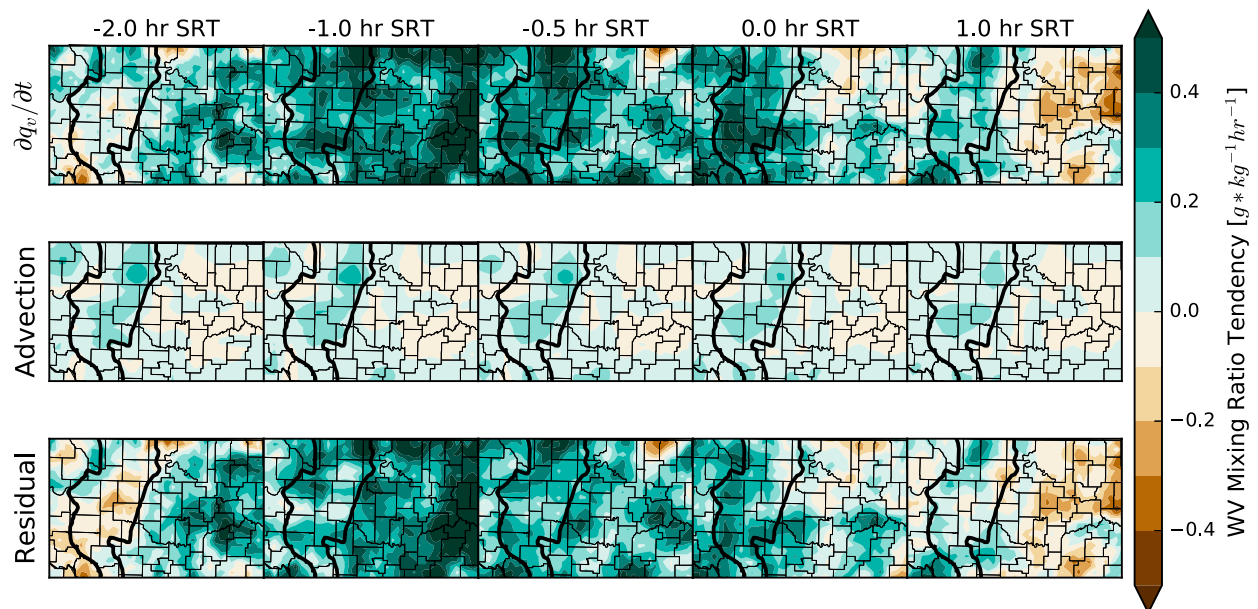


FIG. 8. As in Fig. 7, but for July.

note that the increases observed in the summer months were stronger than those in the spring—a similar result was found in [Wingo and Knupp \(2015\)](#). However, whereas [Wingo and Knupp \(2015\)](#) hypothesized that nighttime increases in q_v were due to evapotranspiration, we find that the increases in near-surface q_v in Oklahoma may be driven by q_v advection and indicate that the relative contributions from evapotranspiration and advection throughout the AET may be very location dependent. In fact, advection appears to better explain some of the postsunset behavior of q_v within the WWB as its value is larger than the residual term (1 h SRT; [Fig. 8](#)). One reason advection dominates may be that downward momentum transfer from the NLLJ enhances the near-surface transport. Another reason may be because the loss of insolation limits the contributions of photosynthesis to evapotranspiration. However, some plants such as wheat may continue to transpire even after insolation has reached zero because they may not close their stomata until long after sunset ([Rawson and Clarke 1988](#)). Future studies may need to perform a closer analysis of plant transpiration behavior with respect to insolation; this could also help to separate out the contributions from the soil versus plants to evapotranspiration during the AET, which our current dataset cannot do. Broadly though, [Fig. 8](#) hints that the loss of convectively generated turbulence during the AET leads to the decoupling of an air mass in both the vertical and lateral directions. In our case, the horizontal q_v gradients developed by the daytime land surface interactions start to become detached from their source regions as mixing decreases and advection becomes more important in the evolution of the moisture field (from -2 to -1 h SRT; [Fig. 8](#)). Future work will be required to continue to understand the relative importance of local and nonlocal processes on AET behavior.

b. Environmental controls on the presunset q_v maximum

It is apparent from the previous analyses that the changes in water vapor occurring prior to sunset can be quite substantial in magnitude and are linked to the land surface properties. We now address the question: What kind of environmental conditions increase the probability of a near-surface water vapor maxima occurring prior to sunset? To better understand the relevant dependencies, the data were tested for sensitivities to soil moisture, ambient wind speeds, and cloud cover. These three variables may be thought of as possible inputs to parameterize the contributions from evapotranspiration. For the soil moisture and AET wind speeds, the average FWI from the 5 cm soil moisture probe and the

wind speed during the 1.5 h prior to sunset were analyzed. For these two environmental variables, the dataset was divided based upon the FWI and wind speed. For FWI, the median FWI value was used as the dividing point to separate AETs as having wet or dry soil. This FWI dividing value of (0.85) is useful in this analysis as a majority of the vegetation in Oklahoma is known to flourish when FWI is above 0.8 ([Flanagan et al. 2017](#)). For wind speed, very slow ($<2 \text{ m s}^{-1}$), slow ($2\text{--}5 \text{ m s}^{-1}$), and fast ($>5 \text{ m s}^{-1}$) categories were used. For the cloud cover variables, the dataset was divided into AETs with clear skies, scattered clouds, and overcast conditions using the logic discussed in [section 2a](#). This analysis strategy was used to test the sensitivity of a presunset q_v maximum to soil moisture, wind speed, and cloud cover. Each of these controls may be considered to be a proxy for the evapotranspiration term in [Eq. \(1\)](#).

These tests suggest that the likelihood of a presunset q_v maxima (cf. [Fig. 6](#)) is strongly dependent on the near-surface wind speed ([Figs. 9a–c](#)). This dependency is most evident in the WWB ([Fig. 9b](#)) and E-WWB ([Fig. 9c](#)) regions and in particular in months when each location has actively growing vegetation. For the WWB sites, the sensitivity to wind speed is largest prior to the winter wheat harvest. For the E-WWB, this sensitivity is present between April and July, with the largest probability differences between AETs with fast and slow winds in May and July. The sensitivities within these time periods and locations are large; the probability differences between each group (even when considering the 95% confidence intervals) are between 10% and 15%. Although the number of samples in the very slow categories are below the minimum number of samples for bootstrapping, this fact does not affect our conclusions. In addition, a similar sensitivity of the presunset jumps in q_v to wind speed was also found in [Acevedo and Fitzjarrald \(2001\)](#) using a simple two-level, one-dimensional diurnal boundary layer model. With this model, they concluded that faster wind speeds during the AET prevents the decoupling of layers near the surface. Their model analysis suggests that only by decoupling the PBL can the contributions from evapotranspiration reach a magnitude large enough to replicate the presunset increase in the near-surface q_v found in observations. Using a multiyear dataset, our results supplement the [Acevedo and Fitzjarrald \(2001\)](#) model by demonstrating with observations that low wind speeds increase the likelihood of a presunset q_v maxima.

It is also apparent that, for all three regions and most months, an increase in soil wetness also increases the probability of a presunset water vapor maxima by 5%–10% ([Figs. 9d–f](#)). For most months in the W-WWB ([Fig. 9d](#)) and WWB regions ([Fig. 9e](#)), the 95% confidence intervals

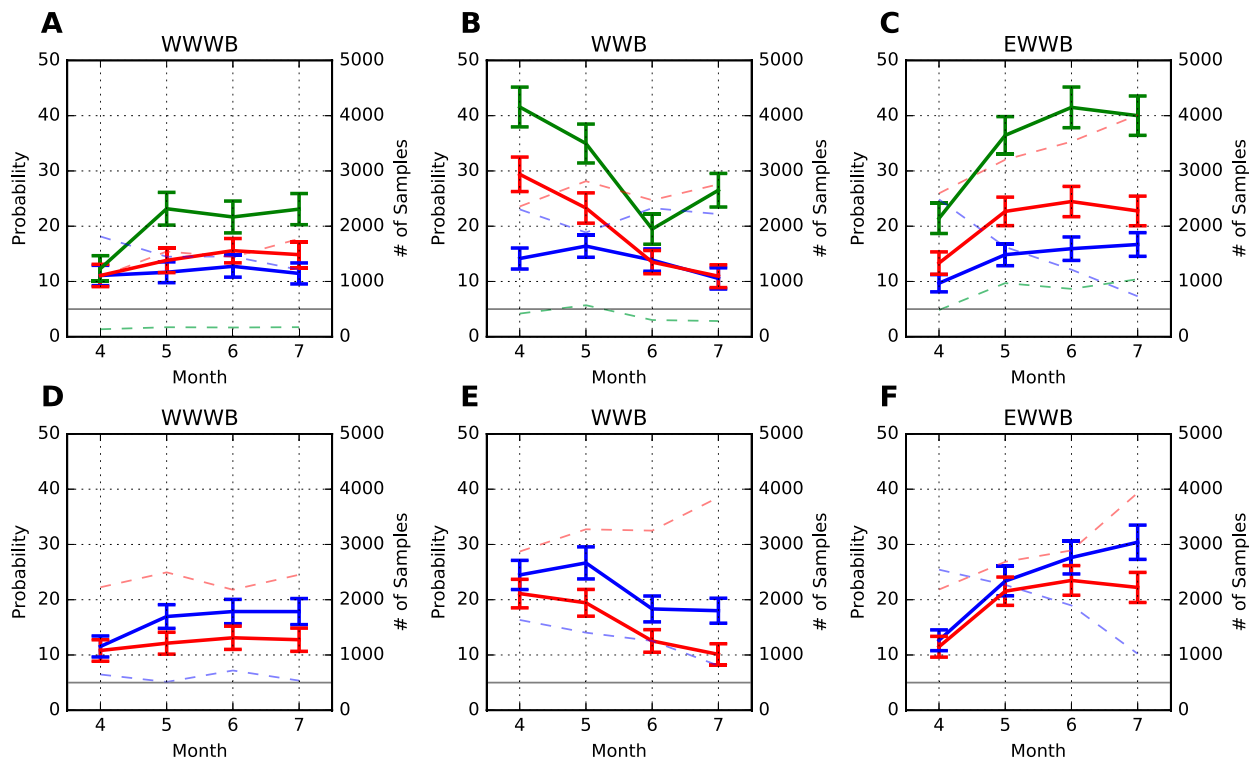


FIG. 9. Plots illustrating how the probability of a q_v maxima prior to sunset is dependent upon (a)–(c) wind speed and (d)–(f) FWI, by month and land-surface region. Solid lines depict the probability of the q_v maximum occurring within 1.5 h prior to sunset. Each panel indicates a WWB-relative region, and the x-axis indicates each month. In (a)–(c), blue indicates AETs for which the wind speed is $> 5 \text{ m s}^{-1}$, red indicates the wind speed is between 2 and 5 m s^{-1} , and green indicates the wind speed is $< 2 \text{ m s}^{-1}$. In (d)–(f), blue indicates the category where the FWI is > 0.85 (i.e., wet soil) and red indicates that FWI is < 0.85 . Error bars indicate the 95% confidence interval of those probabilities, computed by bootstrapping. The dashed lines indicate the number of samples available for bootstrapping, and the horizontal solid gray line indicates the minimum number of samples for bootstrapping (500).

of the two soil wetness categories do not overlap. The shifts in the probability of the presunset q_v maxima over time coincide with the growth of vegetation in the E-WWB region (Fig. 9f) and the start of the harvest along the WWB. These dependencies on soil moisture and vegetation suggest that evapotranspiration is an important factor leading to the presunset AET q_v maxima, as the likelihood of a presunset q_v maxima increases when the soil is relatively wet. Past studies (e.g., Fitzjarrald and Lala 1989; Wingo and Knupp 2015) of the AET in other locations have also suggested that this process may be the primary cause behind the increase in q_v observed during the hours prior to sunset. Combined with past work, our results broadly suggest that evapotranspiration-driven AET q_v jumps may be a part of the coupling known that exists between the land surface and atmosphere in the SGP (Basara and Crawford 2002).

In a final test, the sensitivity of the AET q_v maxima to cloud cover was examined for only the WWB region (Fig. 10). Figure 10 shows that the q_v maxima PDFs for AETs with clear and scattered cloud conditions are

nearly identical in May and June (shown to illustrate the changes before and after the WWB harvest). For both AETs with clear and scattered clouds, there is an increase in the probability of a q_v maximum beginning 1.5 h before sunset in the preharvest months and after sunset in the postharvest months. However, when the skies are overcast, the PDFs for the WV maximum are roughly uniform throughout the entire AET. This behavior suggests that to obtain AETs with a q_v increase after 1.5 h SRT convective eddies driven by insolation must be present during the daytime AET hours. This fact illustrates that one of the key requirements for observing the various processes of the AET (e.g., q_v increase, decrease in wind variance) is that atmospheric turbulence generated convectively must undergo a decay caused by reduced insolation. Although this occurs frequently at the end of each day as a result of sunset, it may also occur in other scenarios (e.g., a solar eclipse; Turner et al. 2018). In addition, another explanation may be that the decrease in solar radiation decreases the surface evapotranspiration.

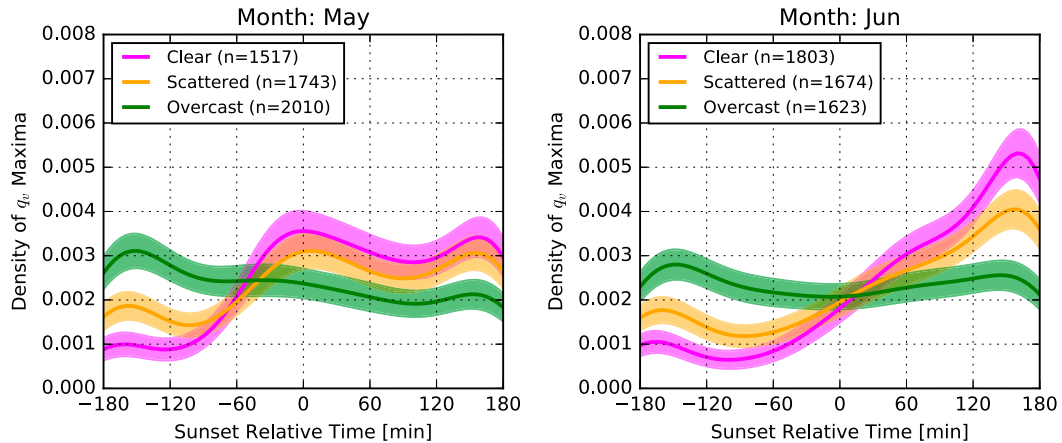


FIG. 10. WWB bootstrapped PDFs for (left) May and (right) June to indicate the likely time that the q_v time series reaches a maximum. This analysis is similar to that in Fig. 6; however, the data shown test the sensitivity to sky cover. Here, pink indicates clear skies, orange indicates scattered skies, and green indicates overcast conditions. See section 3 for information on the sky classification algorithm.

5. Implications on parcel instability and deep, moist convection

The magnitude of the q_v changes found within Oklahoma Mesonet data during the AET suggested that the processes facilitating the change in q_v may increase parcel instability despite the loss of solar heating. This implication is important given the motivation to better understand the behavior of additional ingredients relevant to deep, moist convection during the AET (see section 1). Per the ingredients-based method (Doswell et al. 1996), evidence showing an increase in parcel buoyancy during the AET due to changes in q_v would identify this behavior as a new process that may signal that storm updrafts should intensify around sunset in the SGP. In this final section, evidence for a presunset maximum in instability was sought by asking if a presunset maximum in equivalent potential temperature θ_e also exists.

It is apparent from the data that a maximum in θ_e occurs most often at the beginning of the AET (Fig. 11). Individual time series demonstrate that these maxima are primarily because cooling of the surface layer occurs steadily throughout the AET, which places a virtual temperature maximum at the beginning of the AET (not shown). However, as time progresses during the AET, Fig. 11 shows the parcel θ_e does not always drop off sharply. In fact, many of the individual Mesonet time series (not shown) suggest that local maxima in θ_e may occur 1.5 h prior to sunset and well after sunset. When taken with Fig. 6, this result indicates that the rapid increases in q_v during the AET may also increase the θ_e . This result is notable as it demonstrates that q_v jumps during the AET can reverse the expected loss of the

conditional instability caused by the loss of insolation. To our knowledge, this presunset maxima in θ_e during the AET has not been documented in peer-reviewed literature.

Furthermore, the relative probabilities of a maximum of θ_e are linked to the land surface characteristics (Fig. 11). For each month, WWB-relative locations that have vegetation (indicated by the larger NDVI values in Fig. 1) present exhibit a higher probability of a maximum in conditional instability in the hour and a half preceding sunset. In March and April, the WWB exhibits higher probabilities than the E-WWB or W-WWB categories. In May, there is an increase in the probabilities of the E-WWB category, which is coincident with the growth of vegetation east of the WWB (Fig. 1). After the harvest of the WWB, the E-WWB sites display a higher likelihood of a presunset maximum in θ_e than the other sites (due to the reduction of the probabilities of the WWB category). In addition, a subtle relationship between the land surface and θ_e also appears after sunset in the postharvest months. While small, it appears that the W-WWB and WWB regions exhibit a slightly larger likelihood than the E-WWB region of a θ_e maximum after sunset. This increase in instability is due to the increases in near-surface water vapor that persist after sunset, as was seen in the previous section.

6. Conclusions

By using a 20-yr dataset of Oklahoma Mesonet observations, this study addressed three questions toward understanding the processes and behavior of water vapor changes during the AET in Oklahoma. These

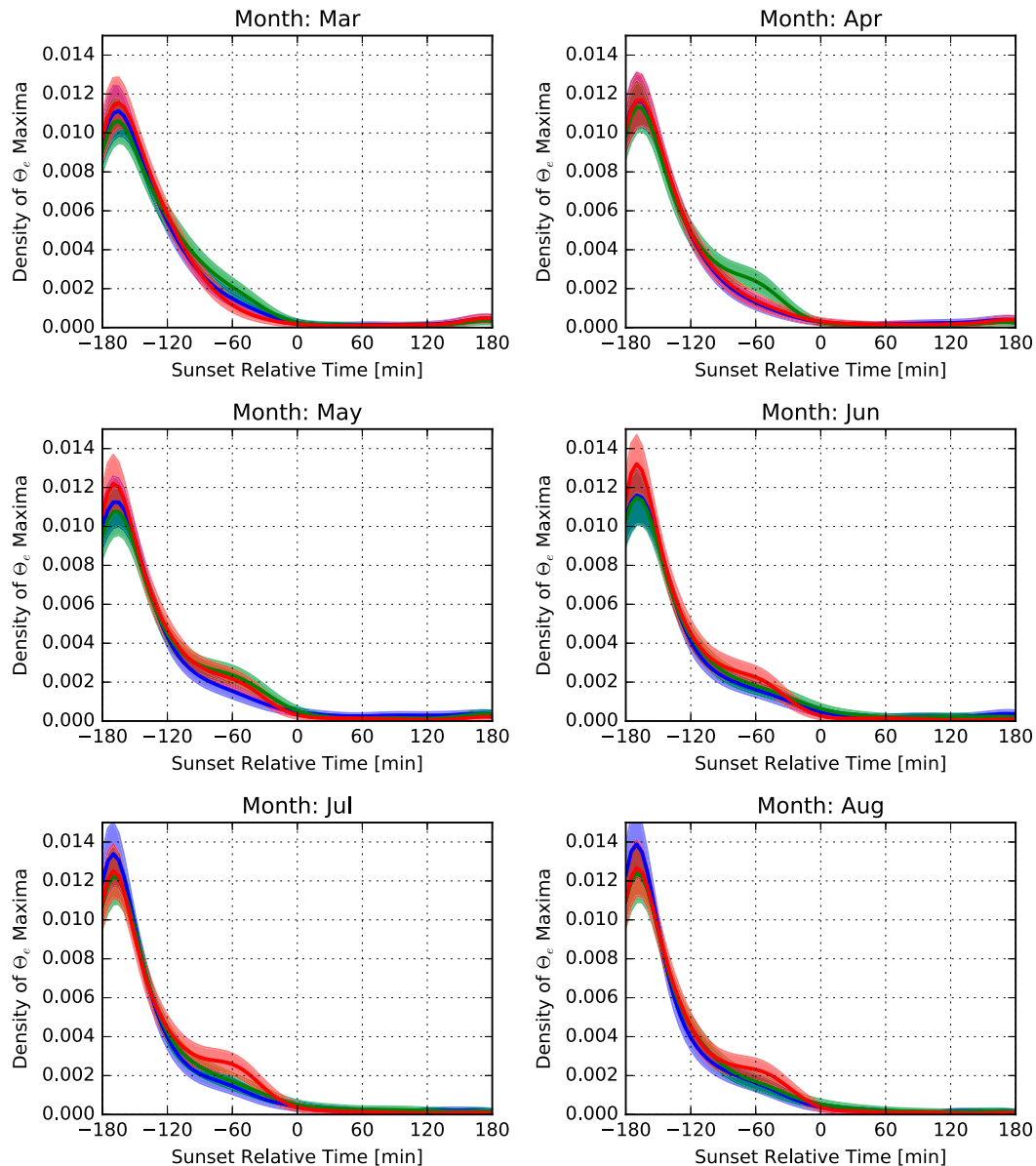


FIG. 11. Similar to Fig. 10, but showing the bootstrapped PDFs indicating the time of maximum θ_e (a proxy for conditional instability).

questions sought to document rapid increases in water vapor q_v occurring during the AET as similar behavior has been documented outside the SGP. By doing so, this study attempted to build upon and synthesize past research encompassing the AET and the SGP discussed in section 1. Two methods were applied to data collected by the Oklahoma Mesonet. In the first, a 2D-VAR algorithm was used to analyze the water vapor and wind field to a grid. In the second, PDFs were generated using the Oklahoma Mesonet data to describe the times during the AET at which q_v reaches a global maximum.

Monthly analyses of this data revealed several findings about the processes and behavior of q_v during Oklahoma AETs. First, the increase in q_v we show are similar to those found in past studies in magnitude and timing (e.g., Wingo and Knupp 2015). However, this research shows that in the SGP q_v behavior is strongly influenced by changes in the land surface, and particularly the annual harvest of winter wheat that occurs from late May through early June. Particularly, the data show that when q_v increases during the AET they are most often found within the WWB. By calculating q_v advection from the 2D-VAR data, we attempted to

estimate the local and nonlocal contributions to the observed water vapor changes. During the months when the winter wheat was still present in Oklahoma (March–May), evidence shows that evapotranspiration is the dominant process within the WWB. After the harvest (June–August), both advection and evapotranspiration facilitate the strong increases over the WWB, while east of the WWB evapotranspiration plays a primary role. The data suggest that advection along the WWB is made possible because the spatial changes in land surface properties (and therefore surface fluxes) brought on by the harvest drive the development of a moisture gradient along the WWB during the daytime. Overall, the dependency on vegetation and vegetation boundaries in these datasets suggest that both evapotranspiration and advection may play important, although location dependent roles in determining the changes of q_v during the AET. Future work will continue to investigate this concept using additional tools.

Sensitivity tests were also performed to better understand the controls on the local contribution by evapotranspiration. Independent variables that act as proxies for the local contribution term were established (e.g., wind speed for mechanical mixing of moisture). These tests revealed that the likelihood of a maximum in q_v during the presunset hours increases when skies are clear, wind speeds are low, and soil moisture is high. Extensions of our study could investigate sensitivities to wind direction, insolation, or recent precipitation and may benefit from an improved detection method to explore potential moisture–AET feedbacks (Sastre et al. 2015). Although our method revealed important consequences and sensitivities of the changes occurring, its focus on global extrema within the AET may mask smaller-amplitude features, such as time series with multiple jumps in q_v . Improved time series analysis and new insights regarding the AET may be revealed by more sophisticated change detection methods such as L1-trend filtering (Kim et al. 2009). This strategy could better quantify the distribution of individual events that occur during the AET that impact water vapor.

Last, a presunset local maximum in conditional instability caused by the AET q_v increase was found. This maximum does not appear to have been identified in past studies. This feature demonstrates that despite the falling near-surface temperatures occurring throughout the AET, a q_v increase can counteract the expected loss of buoyancy caused by reduced surface heating during sunset. Next to known environmental increases in low-level shear (e.g., Maddox 1993), the increases in the moisture and instability ingredients (Doswell et al. 1996)

found demonstrate that AET processes can create other physically significant signals that suggest an increase in the likelihood of deep, moist convection and its related hazards. This notion motivates new questions on the influence of these other environmental changes on deep, moist convection during the AET. Future work studying direct and indirect storm–environment interactions should help also to clarify how and when these various AET processes that modify these different convective ingredients (e.g., shear, moisture) contribute to observed changes in storm behavior (see “6 o’clock magic”; Maddox 1993; Bosart and Bluestein 2008; Bluestein 2015). Until then, the agricultural dependency found in this study may at least help forecasters to better anticipate locations where q_v may increase during the AET (and therefore instability changes) that are known to be associated with nocturnal tornadoes in the central United States (Mead and Thompson 2011). Taken together with past papers on the influence that agriculture has on deep, moist convection (e.g., Carleton et al. 2001, 2008a,b), this study motivates an intriguing line of questioning as to how much regional farming practices in the SGP contribute to the observed increase in thunderstorm hazards during the evening hours.

Acknowledgments. This work was partially supported by the U.S. Department of Energy Atmospheric System Research (ASR) program via Grant DE-SC0014375. Support was also provided by the director of the Cooperative Institute for Mesoscale Meteorological Studies (CIMMS) at the University of Oklahoma. Analyses for this study were performed using computing resources at the University of Oklahoma (OU) Supercomputing Center for Education and Research (OSCER) and the bds2-vm1 computer at Oak Ridge National Laboratory (ORNL). We thank the staff at OSCER and ORNL for their help in using their computing systems. Data processing in this project used Anaconda Python 2.7 and a variety of packages, including Numpy 1.11.2 (Oliphant 2006), Matplotlib 1.5.1 (Hunter 2007), basemap 1.0.7, Scipy 0.18.1 (Jones et al. 2001), IPython 4.1.2 (Pérez and Granger 2007), and MetPy 0.8.0 (May et al. 2017). The Oklahoma Mesonet data used are accessible from the ARM Archive (Gregory 1994, 1998; <https://www.archive.arm.gov/>). We also acknowledge Dr. Andrew Fagg (OU) for his role as the outside member for author Blumberg’s doctoral committee and his early review of this work. Last, we thank our two anonymous reviewers and Kevin Knupp for their comments, which significantly helped us to improve the overall narrative of this article.

REFERENCES

- Acevedo, O. C., and D. R. Fitzjarrald, 2001: The early evening surface-layer transition: Temporal and spatial variability. *J. Atmos. Sci.*, **58**, 2650–2667, [https://doi.org/10.1175/1520-0469\(2001\)058<2650:TEESLT>2.0.CO;2](https://doi.org/10.1175/1520-0469(2001)058<2650:TEESLT>2.0.CO;2).
- American Meteorological Society, 2019: Dryline. *Glossary of Meteorology*, <http://glossary.ametsoc.org/wiki/Dryline>.
- Arritt, R. W., T. D. Rink, M. Segal, D. P. Today, C. A. Clark, M. J. Mitchell, and K. M. Labas, 1997: The Great Plains low-level jet during the warm season of 1993. *Mon. Wea. Rev.*, **125**, 2176–2192, [https://doi.org/10.1175/1520-0493\(1997\)125<2176:TGPLLJ>2.0.CO;2](https://doi.org/10.1175/1520-0493(1997)125<2176:TGPLLJ>2.0.CO;2).
- Bagley, J. E., L. M. Kueppers, D. P. Billesbach, I. N. Williams, S. C. Biraud, and M. S. Torn, 2017: The influence of land cover on surface energy partitioning and evaporative fraction regimes in the U.S. southern Great Plains. *J. Geophys. Res. Atmos.*, **122**, 5793–5807, <https://doi.org/10.1002/2017JD026740>.
- Balling, R. C., Jr., 1985: Warm season nocturnal precipitation in the great plains of the united states. *J. Climate Appl. Meteor.*, **24**, 1383–1387, [https://doi.org/10.1175/1520-0450\(1985\)024<1383:WSNPIT>2.0.CO;2](https://doi.org/10.1175/1520-0450(1985)024<1383:WSNPIT>2.0.CO;2).
- Basara, J. B., and K. C. Crawford, 2002: Linear relationships between root-zone soil moisture and atmospheric processes in the planetary boundary layer. *J. Geophys. Res.*, **107**, 4274, <https://doi.org/10.1029/2001JD000633>.
- , and J. I. Christian, 2018: Seasonal and interannual variability of land–atmosphere coupling across the southern Great Plains of North America using the North American regional reanalysis. *Int. J. Climatol.*, **38**, 964–978, <https://doi.org/10.1002/joc.5223>.
- , J. Christian, R. Wakefield, J. Otkin, E. Hunt, and D. Brown, 2019: The evolution, propagation, and spread of flash drought in the Central United States during 2012. *Environ. Res. Lett.*, **14**, 084025, <https://doi.org/10.1088/1748-9326/ab2cc0>.
- Benjamin, S. G., and Coauthors, 2004: An hourly assimilation–forecast cycle: The RUC. *Mon. Wea. Rev.*, **132**, 495–518, [https://doi.org/10.1175/1520-0493\(2004\)132<0495:AHACTR>2.0.CO;2](https://doi.org/10.1175/1520-0493(2004)132<0495:AHACTR>2.0.CO;2).
- Blackadar, A. K., 1957: Boundary layer wind maxima and their significance for the growth of nocturnal inversions. *Bull. Amer. Meteor. Soc.*, **38**, 283–290, <https://doi.org/10.1175/1520-0477-38.5.283>.
- Bluestein, H. B., 2015: *Severe Convective Storms and Tornadoes: Observations and Dynamics*. Springer, 456 pp.
- , E. W. McCaul, G. P. Byrd, and G. R. Woodall, 1988: Mobile sounding observations of a tornadic storm near the dryline: The Canadian, Texas storm of 7 May 1986. *Mon. Wea. Rev.*, **116**, 1790–1804, [https://doi.org/10.1175/1520-0493\(1988\)116<1790:MSOAT>2.0.CO;2](https://doi.org/10.1175/1520-0493(1988)116<1790:MSOAT>2.0.CO;2).
- , —, —, —, G. Martin, S. Keighton, and L. C. Showell, 1989: Mobile sounding observations of a thunderstorm near the dryline: The Gruver, Texas storm complex of 25 May 1987. *Mon. Wea. Rev.*, **117**, 244–250, [https://doi.org/10.1175/1520-0493\(1989\)117<0244:MSOAT>2.0.CO;2](https://doi.org/10.1175/1520-0493(1989)117<0244:MSOAT>2.0.CO;2).
- , G. S. Romine, R. Rotunno, D. W. Reif, and C. C. Weiss, 2018: On the anomalous counterclockwise turning of the surface wind with time in the plains of the United States. *Mon. Wea. Rev.*, **146**, 467–484, <https://doi.org/10.1175/MWR-D-17-0297.1>.
- Bolton, D., 1980: The computation of equivalent potential temperature. *Mon. Wea. Rev.*, **108**, 1046–1053, [https://doi.org/10.1175/1520-0493\(1980\)108<1046:TCOEPT>2.0.CO;2](https://doi.org/10.1175/1520-0493(1980)108<1046:TCOEPT>2.0.CO;2).
- Bonin, T., P. Chilson, B. Zielke, and E. Fedorovich, 2013: Observations of the early evening boundary-layer transition using a small unmanned aerial system. *Bound.-Layer Meteor.*, **146**, 119–132, <https://doi.org/10.1007/s10546-012-9760-3>.
- Bonner, W. D., 1968: Climatology of the low level jet. *Mon. Wea. Rev.*, **96**, 833–850, [https://doi.org/10.1175/1520-0493\(1968\)096<0833:COTLLJ>2.0.CO;2](https://doi.org/10.1175/1520-0493(1968)096<0833:COTLLJ>2.0.CO;2).
- Bosart, L. F., and H. B. Bluestein, 2008: *Synoptic–Dynamic Meteorology and Weather Analysis and Forecasting: A Tribute to Fred Sanders. Meteor. Monogr.*, No. 33, Amer. Meteor. Soc., 423 pp.
- Brock, F. V., K. C. Crawford, R. L. Elliott, G. W. Cuperus, S. J. Stadler, H. L. Johnson, and M. D. Eilts, 1995: The Oklahoma Mesonet: A technical overview. *J. Atmos. Oceanic Technol.*, **12**, 5–19, [https://doi.org/10.1175/1520-0426\(1995\)012<0005:TOMATO>2.0.CO;2](https://doi.org/10.1175/1520-0426(1995)012<0005:TOMATO>2.0.CO;2).
- Busse, J., and K. Knupp, 2012: Observed characteristics of the afternoon–evening boundary layer transition based on sodar and surface data. *J. Appl. Meteor. Climatol.*, **51**, 571–582, <https://doi.org/10.1175/2011JAMC2607.1>.
- Carleton, A. M., J. Adegoke, J. Allard, D. L. Arnold, and D. J. Travis, 2001: Summer season land cover–convective cloud associations for the Midwest U.S. “Corn Belt. *Geophys. Res. Lett.*, **28**, 1679–1682, <https://doi.org/10.1029/2000GL012635>.
- , D. L. Arnold, D. J. Travis, S. Curran, and J. O. Adegoke, 2008a: Synoptic circulation and land surface influences on convection in the Midwest U.S. “Corn Belt” during the summers of 1999 and 2000. Part I: Composite synoptic environments. *J. Climate*, **21**, 3389–3415, <https://doi.org/10.1175/2007JCLI1578.1>.
- , D. J. Travis, J. O. Adegoke, D. L. Arnold, and S. Curran, 2008b: Synoptic circulation and land surface influences on convection in the Midwest U.S. “Corn Belt” during the summers of 1999 and 2000. Part II: Role of vegetation boundaries. *J. Climate*, **21**, 3617–3641, <https://doi.org/10.1175/2007JCLI1584.1>.
- Coffer, B. E., and M. D. Parker, 2015: Impacts of increasing low-level shear on supercells during the early evening transition. *Mon. Wea. Rev.*, **143**, 1945–1969, <https://doi.org/10.1175/MWR-D-14-00328.1>.
- Cotton, W. R., M. S. Lin, R. L. McAnelly, and C. J. Treback, 1989: A composite model of mesoscale convective complexes. *Mon. Wea. Rev.*, **117**, 765–783, [https://doi.org/10.1175/1520-0493\(1989\)117<0765:ACMOMC>2.0.CO;2](https://doi.org/10.1175/1520-0493(1989)117<0765:ACMOMC>2.0.CO;2).
- Crawford, T. M., and H. B. Bluestein, 1997: Characteristics of dryline passage during COPS-91. *Mon. Wea. Rev.*, **125**, 463–477, [https://doi.org/10.1175/1520-0493\(1997\)125<0463:CODPDC>2.0.CO;2](https://doi.org/10.1175/1520-0493(1997)125<0463:CODPDC>2.0.CO;2).
- Doswell, C. A., H. E. Brooks, and R. A. Maddox, 1996: Flash flood forecasting: An ingredients-based methodology. *Wea. Forecasting*, **11**, 560–581, [https://doi.org/10.1175/1520-0434\(1996\)011<0560:FFFAIB>2.0.CO;2](https://doi.org/10.1175/1520-0434(1996)011<0560:FFFAIB>2.0.CO;2).
- Ferguson C.R., and E. F. Wood, 2011: Observed land–atmosphere coupling from satellite remote sensing and reanalysis. *J. Hydrometeorol.*, **12**, 1221–1254, <https://doi.org/10.1175/2011JHM1380.1>.
- Fitzjarrald, D. R., and G. G. Lala, 1989: Hudson Valley fog environments. *J. Appl. Meteor.*, **28**, 1303–1328, [https://doi.org/10.1175/1520-0450\(1989\)028<1303:HVFE>2.0.CO;2](https://doi.org/10.1175/1520-0450(1989)028<1303:HVFE>2.0.CO;2).
- Flanagan, P. X., J. B. Basara, J. Otkin, and B. G. Illston, 2017: The effect of the dryline and convective initiation on drought evolution over Oklahoma during the 2011 drought. *Adv. Meteor.*, **2017**, 8430743, <https://doi.org/10.1155/2017/8430743>.
- Ford, T. W., A. D. Rapp, and S. M. Quiring, 2015a: Does afternoon precipitation occur preferentially over dry or wet soils in Oklahoma? *J. Hydrometeorol.*, **16**, 874–888, <https://doi.org/10.1175/JHM-D-14-0005.1>.

- , S. M. Quiring, O. W. Frauenfeld, and A. D. Rapp, 2015b: Synoptic conditions related to land–atmosphere interactions and unorganized convection in Oklahoma. *J. Geophys. Res. Atmos.*, **120**, 11 519–11 535, <https://doi.org/10.1002/2015JD023975>.
- , A. D. Rapp, S. M. Quiring, and J. Blake, 2015c: Soil moisture–precipitation coupling: Observations from the Oklahoma Mesonet and underlying physical mechanisms. *Hydrol. Earth Syst. Sci.*, **19**, 3617–3631, <https://doi.org/10.5194/hess-19-3617-2015>.
- Fujita, T., 1970: The Lubbock tornado: A study of suction spots. *Weatherwise*, **23**, 161–173, <https://doi.org/10.1080/00431672.1970.9932888>.
- Gregory, L., 1994: Oklahoma Mesonet (300KM) (updated daily), Southern Great Plains (SGP) External Data (satellites and others) (×1). Subset used: 1 March 1994–31 August 2014, ARM Data Center, accessed 13 November 2017, <https://www.arm.gov/capabilities/instruments/okm>.
- , 1998: Oklahoma Mesonet Soil Moisture (OKMSOIL) (updated daily), Southern Great Plains (SGP) External Data (satellites and others) (X1). Subset used: 1 March 1994–31 August 2014, ARM Data Center, accessed 13 November 2017, <https://www.arm.gov/capabilities/vaps/okmsoil-124>.
- Hane, C. E., 2004: Quiescent and synoptically-active drylines: A comparison based upon case studies. *Meteor. Atmos. Phys.*, **86**, 195–211, <https://doi.org/10.1007/s00703-003-0026-y>.
- , M. E. Baldwin, H. B. Bluestein, T. M. Crawford, and R. M. Rabin, 2001: A case study of severe storm development along a dryline within a synoptically active environment. Part I: Dryline motion and an eta model forecast. *Mon. Wea. Rev.*, **129**, 2183–2204, [https://doi.org/10.1175/1520-0493\(2001\)129<2183:ACSOSS>2.0.CO;2](https://doi.org/10.1175/1520-0493(2001)129<2183:ACSOSS>2.0.CO;2).
- , R. M. Rabin, T. M. Crawford, H. B. Bluestein, and M. E. Baldwin, 2002: A case study of severe storm development along a dryline within a synoptically active environment. Part II: Multiple boundaries and convective initiation. *Mon. Wea. Rev.*, **130**, 900–920, [https://doi.org/10.1175/1520-0493\(2002\)130<0900:ACSOSS>2.0.CO;2](https://doi.org/10.1175/1520-0493(2002)130<0900:ACSOSS>2.0.CO;2).
- Haugland, M. J., and K. C. Crawford, 2005: The diurnal cycle of land–atmosphere interactions across Oklahoma’s winter wheat belt. *Mon. Wea. Rev.*, **133**, 120–130, <https://doi.org/10.1175/MWR-2842.1>.
- Higgins, R. W., Y. Yao, E. S. Yarosh, J. E. Janowiak, and K. C. Mo, 1997: Influence of the Great Plains low-level jet on summertime precipitation and moisture transport over the central United States. *J. Climate*, **10**, 481–507, [https://doi.org/10.1175/1520-0442\(1997\)010<0481:IOTGPL>2.0.CO;2](https://doi.org/10.1175/1520-0442(1997)010<0481:IOTGPL>2.0.CO;2).
- Holton, J. R., 1967: The diurnal boundary layer wind oscillation above sloping terrain. *Tellus*, **19**, 200–205, <https://doi.org/10.3402/tellusa.v19i2.9766>.
- Hunter, J. D., 2007: Matplotlib: A 2D graphics environment. *Comput. Sci. Eng.*, **9**, 90–95, <https://doi.org/10.1109/MCSE.2007.55>.
- Illston, B. G., J. B. Basara, and K. C. Crawford, 2004: Seasonal to interannual variations of soil moisture measured in Oklahoma. *Int. J. Climatol.*, **24**, 1883–1896, <https://doi.org/10.1002/joc.1077>.
- , —, C. A. Fiebrich, K. C. Crawford, E. Hunt, D. K. Fisher, R. Elliott, and K. Humes, 2008: Mesoscale monitoring of soil moisture across a statewide network. *J. Atmos. Oceanic Technol.*, **25**, 167–182, <https://doi.org/10.1175/2007JTECHA993.1>.
- Johnson, Z. F., and N. M. Hitchens, 2018: Effects of soil moisture on the longitudinal dryline position in the southern Great Plains. *J. Hydrometeorol.*, **19**, 273–287, <https://doi.org/10.1175/JHM-D-17-0091.1>.
- Jones, E., and Coauthors, 2001: SciPy: Open source scientific tools for Python. SciPy, <http://www.scipy.org/>.
- Kim, S. J., K. Koh, K. Boyd, and D. Gorinevsky, 2009: L1-trend filtering. *SIAM Rev.*, **51**, 339–360, <https://doi.org/10.1137/070690274>.
- Lothon, M., and Coauthors, 2014: The BLLAST field experiment: Boundary-Layer Late Afternoon and Sunset Turbulence. *Atmos. Chem. Phys.*, **14**, 10 931–10 960, <https://doi.org/10.5194/acp-14-10931-2014>.
- Loveland, T. R., J. W. Merchant, J. F. Brown, D. O. Ohlen, B. C. Reed, P. Olson, and J. Hutchinson, 1995: Seasonal land-cover regions of the United States. *Ann. Assoc. Amer. Geogr.*, **85**, 339–355, <https://doi.org/10.1111/j.1467-8306.1995.tb01798.x>.
- Maddox, R. A., 1980: Mesoscale convective complexes. *Bull. Amer. Meteor. Soc.*, **61**, 1374–1387, [https://doi.org/10.1175/1520-0477\(1980\)061<1374:MCC>2.0.CO;2](https://doi.org/10.1175/1520-0477(1980)061<1374:MCC>2.0.CO;2).
- , 1983: Large-scale meteorological conditions associated with midlatitude mesoscale convective complexes. *Mon. Wea. Rev.*, **111**, 1475–1493, [https://doi.org/10.1175/1520-0493\(1983\)111<1475:LSMCAW>2.0.CO;2](https://doi.org/10.1175/1520-0493(1983)111<1475:LSMCAW>2.0.CO;2).
- , 1993: Diurnal low-level wind oscillation and storm-relative helicity. *The Tornado: Its Structure, Dynamics, Prediction, and Hazards*, *Geophys. Monogr.*, Vol. 79, Amer. Geophys. Union, 591–598.
- Mahrt, L., 1981: The early evening boundary layer transition. *Quart. J. Roy. Meteor. Soc.*, **107**, 329–343, <https://doi.org/10.1002/qj.49710745205>.
- Markowski, P. M., and D. J. Stensrud, 1998: Mean monthly diurnal cycles observed with PRE-STORM surface data. *J. Climate*, **11**, 2995–3009, [https://doi.org/10.1175/1520-0442\(1998\)011<2995:MMDCOW>2.0.CO;2](https://doi.org/10.1175/1520-0442(1998)011<2995:MMDCOW>2.0.CO;2).
- May, R. M., Arms, S. C., Marsh, P., Bruning, E. and Leeman, J. R., 2017: MetPy: A Python Package for Meteorological Data. Unidata, Accessed 31 March 2017, <https://github.com/Unidata/MetPy>.
- McPherson, R. A., and D. J. Stensrud, 2005: Influences of a winter wheat belt on the evolution of the boundary layer. *Mon. Wea. Rev.*, **133**, 2178–2199, <https://doi.org/10.1175/MWR2968.1>.
- , —, and K. C. Crawford, 2004: The Impact of Oklahoma’s winter wheat belt on the mesoscale environment. *Mon. Wea. Rev.*, **132**, 405–421, [https://doi.org/10.1175/1520-0493\(2004\)132<0405:TIOOWW>2.0.CO;2](https://doi.org/10.1175/1520-0493(2004)132<0405:TIOOWW>2.0.CO;2).
- , and Coauthors, 2007: Statewide monitoring of the mesoscale environment: A technical update on the Oklahoma Mesonet. *J. Atmos. Oceanic Technol.*, **24**, 301–321, <https://doi.org/10.1175/JTECH1976.1>.
- Mead, C. M., and R. L. Thompson, 2011: Environmental characteristics associated with nocturnal significant-tornado events in the central and southern Great Plains. *Electron. J. Severe Storms Meteorol.*, **6** (6), <http://www.ejssm.org/ojs/index.php/ejssm/article/viewArticle/84>.
- Means, L. L., 1944: The nocturnal maximum occurrence of thunderstorms in the midwestern states. Master’s thesis, Dept. of Physics, University of Chicago, 38 pp.
- , 1954: A study of the mean southerly wind maximum in low levels associated with a period of summer precipitation in the Middle West. *Bull. Amer. Meteor. Soc.*, **35**, 166–170, <https://doi.org/10.1175/1520-0477-35.4.166>.
- Oliphant, T. E., 2006: *A Guide to NumPy*. Trelgol Publishing, 261 pp.
- Orville, R. E., 1981: Global distribution of midnight lightning—September to November 1977. *Mon. Wea. Rev.*, **109**, 391–395,

- [https://doi.org/10.1175/1520-0493\(1981\)109<0391:GDOMLT>2.0.CO;2](https://doi.org/10.1175/1520-0493(1981)109<0391:GDOMLT>2.0.CO;2).
- Parsons, D. B., M. A. Shapiro, R. M. Hardesty, R. J. Zamora, and J. M. Intrieri, 1991: The finescale structure of a west Texas dryline. *Mon. Wea. Rev.*, **119**, 1242–1258, [https://doi.org/10.1175/1520-0493\(1991\)119<1242:TFSOAW>2.0.CO;2](https://doi.org/10.1175/1520-0493(1991)119<1242:TFSOAW>2.0.CO;2).
- Pérez, F., and B. E. Granger, 2007: IPython: A system for interactive scientific computing. *Comput. Sci. Eng.*, **9**, 21–29, <https://doi.org/10.1109/MCSE.2007.53>.
- Pitchford, K. L., and J. London, 1962: The low-level jet as related to nocturnal thunderstorms over the midwest United States. *J. Appl. Meteor.*, **1**, 43–47, [https://doi.org/10.1175/1520-0450\(1962\)001<0043:TLLJAR>2.0.CO;2](https://doi.org/10.1175/1520-0450(1962)001<0043:TLLJAR>2.0.CO;2).
- Purser, R. J., W.-S. Wu, D. F. Parrish, and N. M. Roberts, 2003: Numerical aspects of the application of recursive filters to variational statistical analysis. Part I: Spatially homogeneous and isotropic Gaussian covariances. *Mon. Wea. Rev.*, **131**, 1524–1535, [https://doi.org/10.1175/1520-0493\(2003\)131<1524:NAOTAO>2.0.CO;2](https://doi.org/10.1175/1520-0493(2003)131<1524:NAOTAO>2.0.CO;2).
- Rabin, R. M., S. Stadler, P. J. Wetzel, D. J. Stensrud, and M. Gregory, 1990: Observed effects of landscape variability on convective clouds. *Bull. Amer. Meteor. Soc.*, **71**, 272–280, [https://doi.org/10.1175/1520-0477\(1990\)071<0272:OEOLVO>2.0.CO;2](https://doi.org/10.1175/1520-0477(1990)071<0272:OEOLVO>2.0.CO;2).
- Rawson, H. M., and J. M. Clarke, 1988: Nocturnal transpiration in wheat. *Funct. Plant Biol.*, **15**, 397–406, <https://doi.org/10.1071/PP9880397>.
- Rhodes, B. C., 2011: Pyephem: Astronomical ephemeris for python, <http://adsabs.harvard.edu/abs/2011ascl.soft12014R>.
- Ruiz-Barradas, A., and S. Nigam, 2013: Atmosphere–land surface interactions over the southern Great Plains: Characterization from pentad analysis of DOE ARM field observations and NARR. *J. Climate*, **26**, 875–886, <https://doi.org/10.1175/JCLI-D-11-00380.1>.
- Santanello, J. A., Jr., C. D. Peters-Lidard, S. V. Kumar, C. Alonge, and W.-K. Tao, 2009: A modeling and observational framework for diagnosing local land–atmosphere coupling on diurnal time scales. *J. Hydrometeorol.*, **10**, 577–599, <https://doi.org/10.1175/2009JHM1066.1>.
- , —, and —, 2011: Diagnosing the sensitivity of local land–atmosphere coupling via the soil moisture–boundary layer interaction. *J. Hydrometeorol.*, **12**, 766–786, <https://doi.org/10.1175/JHM-D-10-05014.1>.
- , —, A. Kennedy, and S. V. Kumar, 2013: Diagnosing the nature of land–atmosphere coupling: A case study of dry/wet extremes in the U.S. southern Great Plains. *J. Hydrometeorol.*, **14**, 3–24, <https://doi.org/10.1175/JHM-D-12-023.1>.
- , J. Roundy, and P. A. Dirmeyer, 2015: Quantifying the land–atmosphere coupling behavior in modern reanalysis products over the U.S. southern Great Plains. *J. Climate*, **28**, 5813–5829, <https://doi.org/10.1175/JCLI-D-14-00680.1>.
- Sastre, M., C. Yagüe, C. Román-Cascón, and G. Maqueda, 2015: Atmospheric boundary-layer evening transitions: A comparison between two different experimental sites. *Bound.-Layer Meteorol.*, **157**, 375–399, <https://doi.org/10.1007/s10546-015-0065-1>.
- Schaefer, J. T., 1974: The life cycle of the dryline. *J. Appl. Meteorol.*, **13**, 444–449, [https://doi.org/10.1175/1520-0450\(1974\)013<0444:TLCOTD>2.0.CO;2](https://doi.org/10.1175/1520-0450(1974)013<0444:TLCOTD>2.0.CO;2).
- Scott, D. W., 2015: *Multivariate Density Estimation: Theory, Practice, and Visualization*. John Wiley and Sons, 384 pp.
- Shapiro, A., E. Fedorovich, and S. Rahimi, 2016: A unified theory for the Great Plains nocturnal low-level jet. *J. Atmos. Sci.*, **73**, 3037–3057, <https://doi.org/10.1175/JAS-D-15-0307.1>.
- Spencer, P. L., and C. A. Doswell III, 2001: A quantitative comparison between traditional and line integral methods of derivative estimation. *Mon. Wea. Rev.*, **129**, 2538–2554, [https://doi.org/10.1175/1520-0493\(2001\)129<2538:AQCBTA>2.0.CO;2](https://doi.org/10.1175/1520-0493(2001)129<2538:AQCBTA>2.0.CO;2).
- , and J. Gao, 2004: Can gradient information be used to improve variational objective analysis? *Mon. Wea. Rev.*, **132**, 2977–2994, <https://doi.org/10.1175/MWR2833.1>.
- , D. J. Stensrud, and J. M. Fritsch, 2003: A method for improved analyses of scalars and their derivatives. *Mon. Wea. Rev.*, **131**, 2555–2576, [https://doi.org/10.1175/1520-0493\(2003\)131<2555:AMFIAO>2.0.CO;2](https://doi.org/10.1175/1520-0493(2003)131<2555:AMFIAO>2.0.CO;2).
- Stensrud, D. J., 1996: Importance of low-level jets to climate: A review. *J. Climate*, **9**, 1698–1711, [https://doi.org/10.1175/1520-0442\(1996\)009<1698:IOLLJT>2.0.CO;2](https://doi.org/10.1175/1520-0442(1996)009<1698:IOLLJT>2.0.CO;2).
- Stull, R. B., 1988: *An Introduction to Boundary Layer Meteorology*. Kluwer Academic, 666 pp.
- Trier, S. B., C. A. Davis, D. A. Ahijevych, M. L. Weisman, and G. H. Bryan, 2006: Mechanisms supporting long-lived episodes of propagating nocturnal convection within a 7-day WRF Model simulation. *J. Atmos. Sci.*, **63**, 2437–2461, <https://doi.org/10.1175/JAS3768.1>.
- , —, and R. E. Carbone, 2014: Mechanisms governing the persistence and diurnal cycle of a heavy rainfall corridor. *J. Atmos. Sci.*, **71**, 4102–4126, <https://doi.org/10.1175/JAS-D-14-0134.1>.
- Turner, D. D., V. Wulfmeyer, A. Behrendt, T. A. Bonin, A. Choukulkar, R. K. Newsom, W. A. Brewer, and D. R. Cook, 2018: Response of the land–atmosphere system over north-central Oklahoma during the 2017 eclipse. *Geophys. Res. Lett.*, **45**, 1668–1675, <https://doi.org/10.1002/2017GL076908>.
- Wakefield, R. A., J. B. Basara, J. C. Furtado, B. G. Illston, C. R. Ferguson, and P. M. Klein, 2019: A modified framework for quantifying land–atmosphere covariability during hydrometeorological and soil wetness extremes in Oklahoma. *J. Appl. Meteor. Climatol.*, **58**, 1465–1483, <https://doi.org/10.1175/JAMC-D-18-0230.1>.
- Wallace, J. M., 1975: Diurnal variations in precipitation and thunderstorm frequency over the conterminous United States. *Mon. Wea. Rev.*, **103**, 406–419, [https://doi.org/10.1175/1520-0493\(1975\)103<0406:DVIPAT>2.0.CO;2](https://doi.org/10.1175/1520-0493(1975)103<0406:DVIPAT>2.0.CO;2).
- Wei, J., R. E. Dickinson, and H. Chen, 2008: A negative soil moisture–precipitation relationship and its causes. *J. Hydrometeorol.*, **9**, 1364–1376, <https://doi.org/10.1175/2008JHM955.1>.
- Wexler, H., 1961: A boundary layer interpretation of the low-level jet. *Tellus*, **13**, 368–378, <https://doi.org/10.3402/tellusa.v13i3.9513>.
- Wingo, S. M., and K. R. Knupp, 2015: Multi-platform observations characterizing the afternoon-to-evening transition of the planetary boundary layer in northern Alabama, USA. *Bound.-Layer Meteorol.*, **155**, 29–53, <https://doi.org/10.1007/s10546-014-9988-1>.
- Zhang, D., and R. A. Anthes, 1982: A high-resolution model of the planetary boundary layer—Sensitivity tests and comparisons with SESAME-79 data. *J. Appl. Meteorol.*, **21**, 1594–1609, [https://doi.org/10.1175/1520-0450\(1982\)021<1594:AHMOT>2.0.CO;2](https://doi.org/10.1175/1520-0450(1982)021<1594:AHMOT>2.0.CO;2).